Zeitschrift: Schweizerische mineralogische und petrographische Mitteilungen = Bulletin suisse de minéralogie et pétrographie

Band: 81 (2001)

Heft: 3: Monte Rosa nappe

Artikel: A retrograde monazite-forming reaction in bearthite-bearing high-pressure rocks

Autor: Scherrer, N.C. / Gnos, E. / Chopin, C.

DOI: https://doi.org/10.5169/seals-61698

SCHWEIZ. MINERAL. PETROGR. MITT. 81, 369–378, 2001

A retrograde monazite-forming reaction in bearthite-bearing high-pressure rocks

by *N.C. Scherrer*[1], *E. Gnos*[1] and *C. Chopin*[2]

Abstract

Bearthite, $Ca_2Al[PO_4]_2(OH)$, an aluminium phosphate that may contain up to ~10 wt% of light rare-earth elements (LREE) + Th, shows various breakdown textures in high-pressure metamorphic rocks. Two such reactions are described: (1) a pyrope-bearing kyanite-phengite-quartz (coesite) schist from the high-pressure Dora-Maira terrane, Italy, in which bearthite displays a symplectitic rim that consists of apatite + monazite; (2) a garnet-bearing muscovite-biotite gneiss of the Monte Rosa nappe, Italy, in which a symplectitic pseudomorph consisting of apatite + corundum + monazite occurs as an inclusion in allanite. In rocks with a high Al/Ca ratio, we suggest that bearthite is more stable than monazite as the LREE-bearing phase under high P/low T conditions (that is, a subduction zone environment). It breaks down to an assemblage of symplectitic monazite + apatite + corundum (or Al-silicate with free SiO_2) during decompression. Bearthite that coexists with HREE-dominated minerals like xenotime does not show increased HREE contents. Because of its considerable Th-content, bearthite could be used to constrain the time of high-pressure metamorphism.

Keywords: bearthite, monazite, metamorphic reaction, EMPA, LREE.

Introduction

Monazite is widely used for age dating in a variety of igneous, metamorphic and diagenetic rocks. There is, however, relatively little knowledge of its formation conditions in metamorphic rocks and, so far, there are only few monazite-forming reactions described in the literature (AKERS, 1993; BINGEN, 1996; BROSKA, 1998; FINGER, 1998; PAN, 1997; SMITH, 1990). This research describes a new reaction observed in retrogressivly overprinted high-pressure rocks: bearthite decays to monazite + apatite + corundum.

CHOPIN et al. (1993) found bearthite, $(Ca,REE,Th,U)_2(PO_4)_2OH$, with symplectitic rims (Fig. 1) of *"apatite containing highly refringent blebs of a rare-earth phosphate (monazite?)"* in metapelites and magnesian schists of the coesite-bearing Dora-Maira terrane. The mineral had previously been observed also in the Monte Rosa nappe (BEARTH, 1952). Recent studies on metapelitic rocks of the Monte Rosa nappe revealed patches of fine-grained and closely intergrown apatite + monazite + corundum, making up the core of a millimetre-sized allanite grain (Fig. 2). Reintegration of microprobe data from the three different minerals that formed the fine-grained areas suggests a precursor rich in LREE with Al as a major component to account for the formation of corundum. The above observations led to the idea that the phosphate bearthite could be a major reactant in a retrogressive monazite-forming reaction in high- or ultra-high-pressure rocks, even though bearthite relics were not observed in this particular sample. For this purpose we re-investigated the symplectitic reaction rim described in CHOPIN et al. (1993), as well as samples from other bearthite localities, and used the REE + Th + U concentrations of bearthite, monazite and apatite in support of the proposed reaction.

[1] Institute of Mineralogy and Petrology, University of Bern, Baltzerstr. 1, CH-3012 Bern. <scherrer@mpi.unibe.ch> <gnos@mpi.unibe.ch>

[2] Laboratoire de Géologie, Ecole normale supérieure, 24 rue Lhomond, F-75005 Paris. <chopin@geologie.ens.fr>

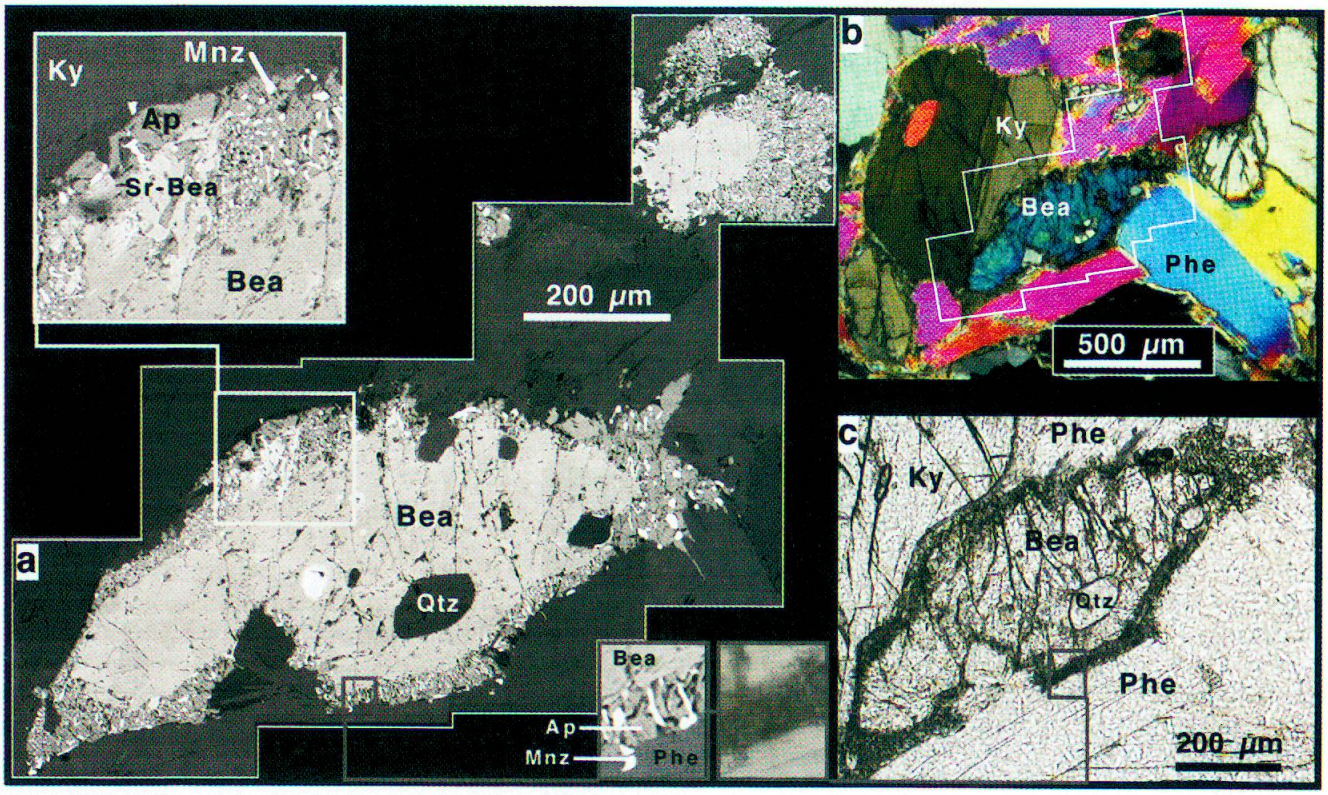

Fig. 1a Symplectitic rim of apatite + monazite around a bearthite grain within a garnet–kyanite–phengite–quartz schist from Dora-Maira, sample 85DM45a. (a) BSE images; the zoom-window of the BSE-map (top left) highlights the presence of Sr-bearthite, which appears to be restricted to the resorbing edge of bearthite, against the symplectite rim. (b) Optical image with crossed polarisers. (c) Optical image with parallel polarisers. Electron microprobe analyses are listed in Tab. 1. Ap = Apatite; Bea = Bearthite; Ky = Kyanite; Mnz = Monazite; Phe = Phengite; Qtz = Quartz.

Samples and sample localities

CHOPIN et al. (1991; 1993, samples 85DM45a and 93-13-1, deposited under No. 27341 at the Mineralogische Staatssammlung, München) discovered bearthite in coesite-bearing rocks of the Dora-Maira terrane. Bearthite occurs as an accessory mineral in metapelitic rocks, as well as in pyrope-bearing kyanite-phengite-quartz (coesite) schists. Symplectitic rims (Fig. 1) composed of apatite + monazite (Tab. 1) have been interpreted as a retrogressive and decompression-related feature (CHOPIN et al. 1993).

No bearthite relics were observed in the sample from the Monte Rosa nappe (Passo del Mottone, south of Antronapiana, sample Mo9801). However, a garnet-bearing two mica gneiss that belongs to the metapelitic, pre-Permian basement, contains a reaction texture of symplectitic apatite + monazite + corundum, enclosed by allanite. Although sillimanite has been observed elsewhere in this rock unit (BEARTH, 1957), no Al-silicate is present in our sample. The sample is a typical garnet-bearing muscovite-biotite gneiss with plagioclase ($Ab_{70}An_{30}$), K-feldspar, quartz and late chlorite as the main constituents. Rutile rimmed by ilmenite is observed primarily as inclusions in garnet, and rarely in the matrix. Phengitic mica ($Mg_{0.29}Si_{3.40}Al_{2.20}$) is present as inclusions in allanite (Fig. 2), but not in the matrix, where only muscovite ($Mg_{0.07}Si_{3.05}Al_{2.80}$) is found. Several large allanite grains, as well as minor apatite and rare monazite are present in this thin section. The samples were collected from the lowest part of the Monte Rosa nappe, within a few metres of the contact with the Antrona trough units (ophiolitic sequence).

As third example (B8485A) of bearthite we examined a sample from the Stockhorngrat (BEARTH, 1952), the type locality of bearthite. Here, bearthite occurs associated with lazulite, apatite, paragonite and xenotime in quartz veins that run parallel to the foliation of the surrounding quartz-phengite schist. In contrast to the previously described samples, the Stockhorngrat bearthite contains virtually no REE and monazite appears to be absent in the thin sections examined. The HREE fractionating phase xenotime was found instead and seems to be the main REE-bearing phase in this sample.

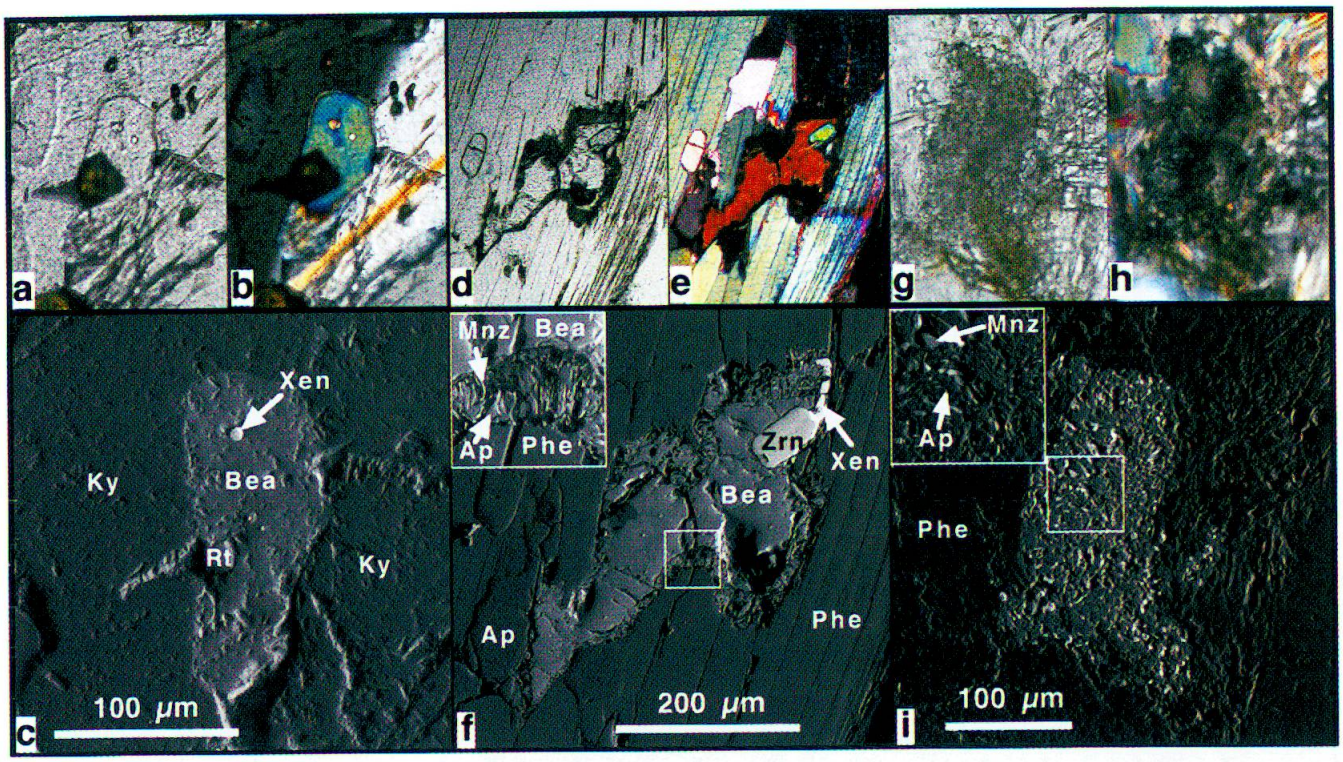

Fig. 1b A succession of bearthite replacement documented within thin sections of sample 85DM45: (a–c) fully intact bearthite grain with sharp contacts to the surrounding minerals; (d–f) bearthite grain with fuzzy contacts to the surrounding minerals, displaying a rim of symplectitic monazite + apatite, similar to Fig. 1a; (g–i) symplectitic monazite + apatite after bearthite (bearthite fully replaced). (a, d, g): parallel polarisers; (b, e, h): crossed polarisers; (c, f, i): BSE images. Rt = Rutile; Xen = Xenotime; Zrn = Zircon.

Methods

An electron microprobe (Cameca SX50 model, at both MPI Bern and IMP Lausanne) was used to produce back-scattered electron (BSE) images, X-ray maps and quantitative analyses. Monazite analyses were performed using electron beam conditions of 25 kV and 50 nA. A detailed description of analytical settings is given in SCHERRER et al. (2000). For bearthite analysis, the same conditions were used, except that the beam current was reduced to 20 or 15 nA, and the beam spot enlarged to ~20 × 20 µm to avoid damage to the bearthite during analysis.

The software NIH Image was used for semi-quantitative analysis of X-ray maps and BSE images to determine the relative amounts of apatite, monazite and corundum within the reaction texture. BSE imaging turned out to be more suitable for this purpose than element maps. Several representative areas were selected to calculate the amount of each phase in 2D.

The fine-grained nature of the symplectitic textures was an additional obstacle to obtaining good analyses. Nevertheless, the original suggestion of CHOPIN et al. (1993) of a symplectite of apatite plus monazite has now been confirmed by quantitative analyses of the monazite in the symplectite (Tab. 1).

Results

Dora-Maira terrane (Sample 85DM45a): Several bearthite grains within this sample, a pyrope-bearing kyanite–phengite–quartz schist (CHOPIN et al. 1993), were mapped in BSE mode to display the different phases present in the symplectite. The symplectites appear to be reaction zones surrounding bearthite, and consist of apatite + monazite (Figs 1a–c). Figure 1a revealed an additional phase that was produced by the symplectite-forming reaction, appearing to be strontian bearthite (Tab. 1). The ratios REE_{Bea}/REE_{Mnz} (i.e. $La_{Bea}/La_{Mnz} \approx Ce_{Bea}/Ce_{Mnz} \approx Nd_{Bea}/Nd_{Mnz} \approx \ldots$) are constant, and none of these elements is present in apatite within the symplectite other than in trace amounts. LREE are thus strongly fractionated into monazite (Figs 3a, d). The REE and Th contents of bearthite are generally 10–20% of those of monazite. Strontian bearthite forms overgrowth patches along the inner side of the symplectite (Fig. 1a) and is present only in direct contact with bearthite. In the symplectite, the esti-

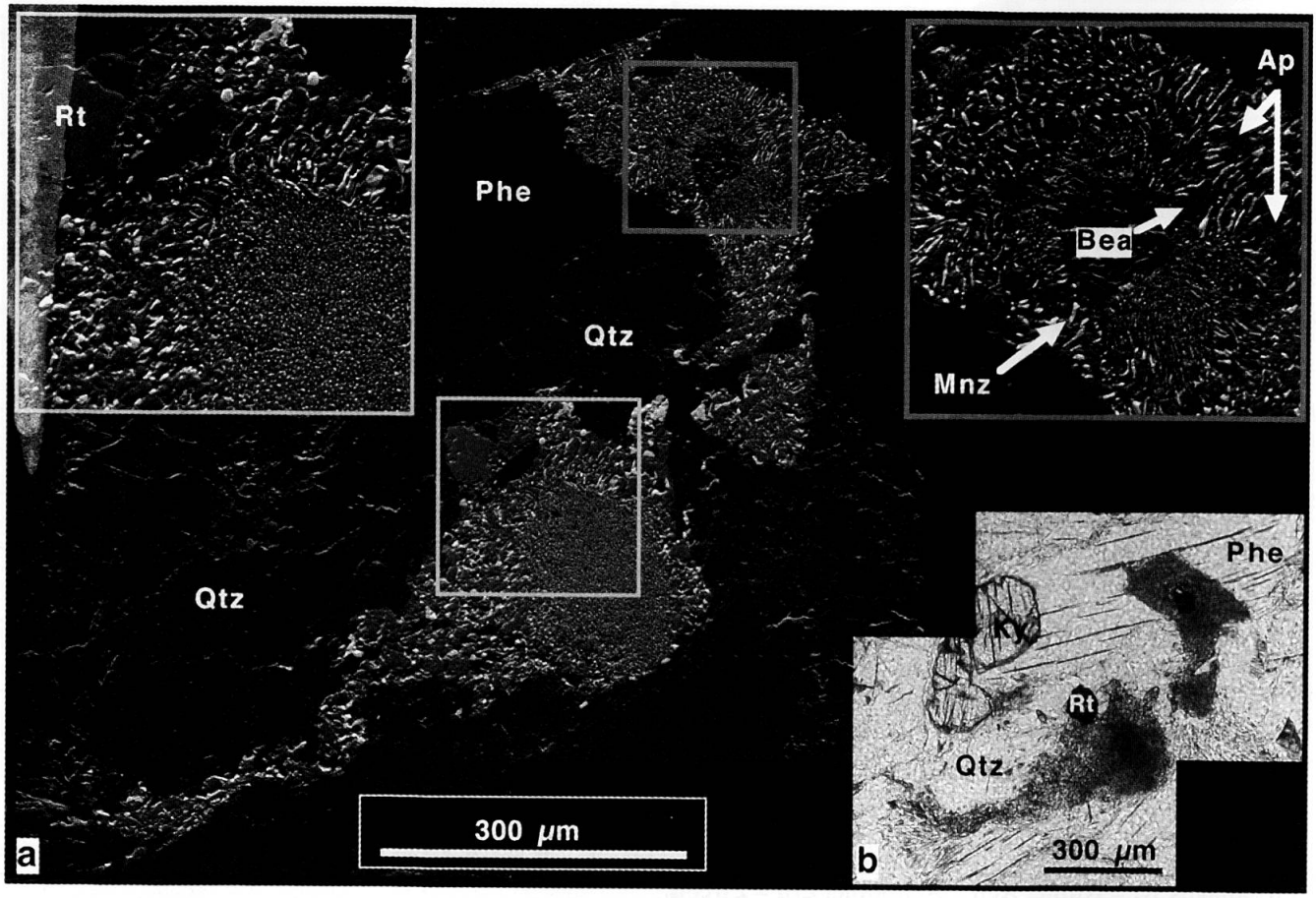

Fig. 1c Example within section 85DM45a where symplectites have almost completely replaced the original beartite. (a) BSE image; (b) optical image with parallel polarisers.

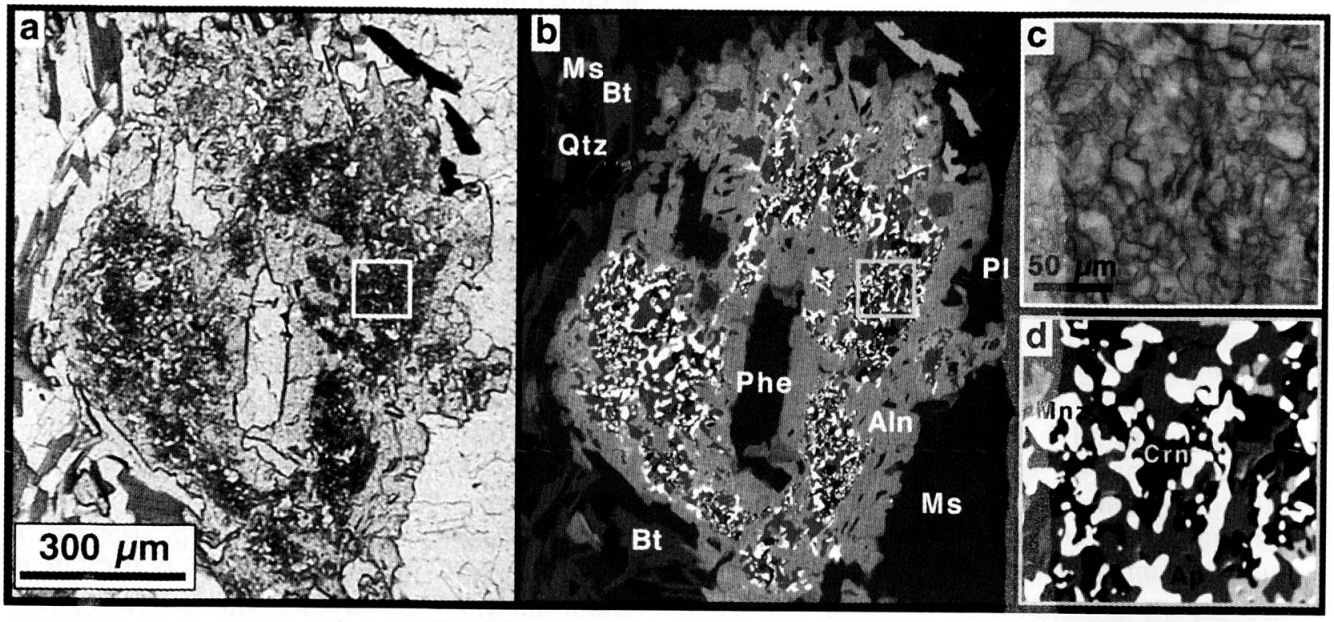

Fig. 2 Optical (a, c) and BSE images (b, d) of sample Mo9801 showing the fine-grained symplectite apatite + monazite + corundum within a large grain of allanite. The close-up view of the BSE image shows that within the reaction zones, allanite is virtually absent. These textural relationships as well as the lack of Si, Fe and Mg within the product phase assemblage suggest that allanite was not involved in the symplectite-forming reaction. Note that the white mica enclosed in the core of the allanite has a phengitic composition ($Mg_{0.29}Si_{3.40}Al_{2.20}$), whereas only muscovite is present in the matrix ($Mg_{0.07}Si_{3.05}Al_{2.80}$). Aln = Allanite; Bt = Biotite; Crn = Corundum; Ms = Muscovite; Pl = Plagioclase.

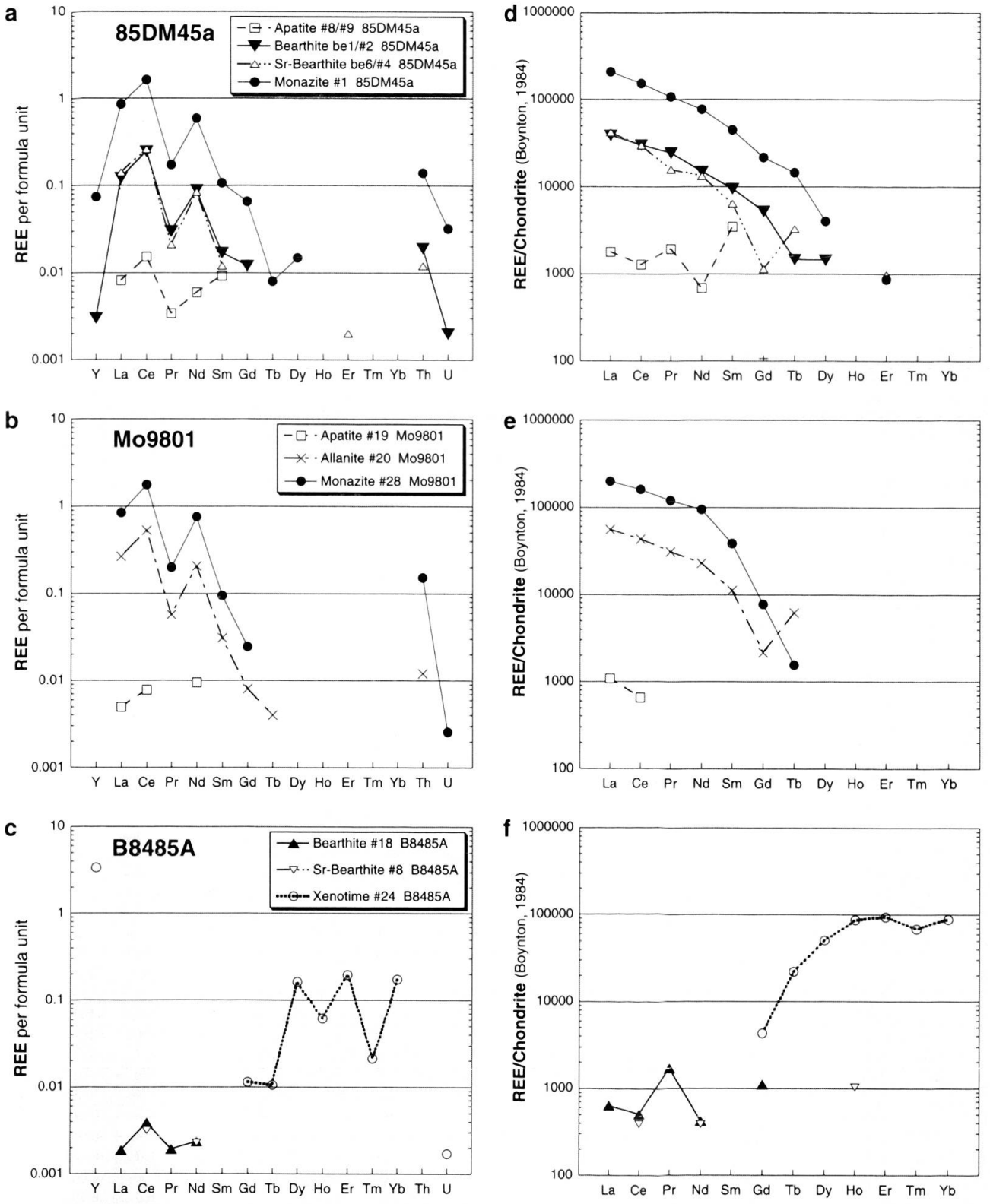

Fig. 3 Series 1 (a, b, c; data from Tab. 1): REE, Th and U concentrations of coexisting phases in samples 85DM45a (a, d), Mo9801 (b, e) and B8485A (c, f). Note the similarity of the REE patterns between the phases of the first two examples, and the completely different element distribution of xenotime against bearthite and Sr-bearthite in B8485A. No monazite was detected in this latter sample. Since bearthite is a reactant in a monazite-forming reaction and has the capacity to incorporate considerable amounts of Th (as shown in example a), mass-spectrometric dating of bearthite offers a new option to derive valuable time-constraints to better understand the genesis of high pressure rocks. Series 2 (d, e, f): the same dataset as on left, using chondrite normalisation values of Boynton (1984). The relative analytical uncertainties (1 σ) for measurements on bearthite are: La, Ce, Nd < 2%; Th < 5%; Sm, Gd < 10%; Pr < 15%; U, Y, Dy < 35%; Tb, Er, Yb ≈ 75–250%. Relative uncertainties are smaller for monazite and xenotime, similar for allanite, and larger for apatite.

Tab. 1

Location	Passo del Mottone, S of Antronapiana					Dora-Maira						Stockhorngrat, SE of Zermatt			
Sample	**Mo9801**					**85DM45a**						**B8485A**			
Mineral	Apatite	Allanite		Monazite		Apatite		Bearthite		Sr-Bearthite	Monazite	Bearthite	Sr-Bearthite	Xenotime	D.L. (2σ)
Point#	#19	#20	#22	#28	#34	#8#9	be1/#2	be2/#2	be3/#4	be6/#4	#1	#18	#8	#24	ppm
P_2O_5	41.97	0.05	29.99	29.64	29.49	41.34	39.68	39.68	42.07	37.61	31.05	43.18	40.75	35.36	400
SiO_2	b.d.	34.16	0.23	0.42	0.93	0.08	0.44	0.50	0.42	0.19	0.23	b.d.	b.d.	b.d.	350
TiO_2	n.a.	0.05	n.a.	n.a.	n.a.	n.a.	n.a.	n.a.	n.a.	n.a.	n.a.	n.a.	n.a.	n.a.	250
Al_2O_3	b.d.	23.67	b.d.	b.d.	b.d.	b.d.	10.78	10.59	12.46	10.10	b.d.	15.55	14.61	b.d.	350
FeO	0.04	7.28	b.d.	b.d.	b.d.	b.d.	b.d.	b.d.	b.d.	b.d.	b.d.	0.07	0.04	b.d.	250
MnO	n.a.	b.d.	n.a.	n.a.	n.a.	n.a.	b.d.	b.d.	b.d.	b.d.	n.a.	n.a.	n.a.	n.a.	300
MgO	n.a.	0.76	n.a.	n.a.	n.a.	2.09	3.02	3.32	2.45	2.82	n.a.	0.30	0.12	b.d.	400
CaO	54.16	13.92	0.33	1.01	1.65	50.91	22.86	23.39	29.02	14.26	1.69	22.82	16.25	0.07	250
SrO	n.a.	n.a.	n.a.	n.a.	n.a.	1.65	6.57	4.73	b.d.	20.34	n.a.	16.07	26.46	b.d.	450
Y_2O_3	b.d.	b.d.	b.d.	b.d.	b.d.	n.a.	0.05	0.11	0.54	b.d.	0.91	b.d.	b.d.	46.77	250
La_2O_3	0.08	4.08	18.09	14.39	11.58	0.13	2.81	3.56	1.81	3.06	15.08	0.05	b.d.	b.d.	200
Ce_2O_3	0.13	8.15	34.23	30.39	26.95	0.24	5.67	6.47	3.86	5.66	29.12	0.10	0.07	b.d.	200
Pr_2O_3	b.d.	0.89	3.40	3.45	3.35	0.06	0.70	0.55	0.30	0.45	3.07	0.05	b.d.	b.d.	500
Nd_2O_3	0.15	3.23	11.03	13.27	14.04	0.10	2.08	2.30	1.47	1.84	10.85	0.06	0.05	b.d.	450
Sm_2O_3	b.d.	0.51	1.20	1.73	2.24	0.16	0.43	0.40	0.27	0.29	2.02	b.d.	b.d.	b.d.	900
Gd_2O_3	b.d.	0.13	0.33	0.46	0.65	b.d.	0.31	0.31	0.30	b.d.	1.29	b.d.	b.d.	0.26	1000
Tb_2O_3	b.d.	0.07	b.d.	b.d.	b.d.	n.a.	b.d.	b.d.	b.d.	b.d.	0.16	b.d.	b.d.	0.24	500
Dy_2O_3	b.d.	b.d.	b.d.	b.d.	b.d.	n.a.	0.11	b.d.	0.13	b.d.	0.30	b.d.	b.d.	3.74	1100
Ho_2O_3	b.d.	b.d.	b.d.	b.d.	b.d.	n.a.	b.d.	b.d.	b.d.	b.d.	b.d.	b.d.	0.02	1.43	900
Er_2O_3	b.d.	b.d.	b.d.	b.d.	b.d.	n.a.	b.d.	b.d.	b.d.	0.05	b.d.	b.d.	b.d.	4.53	500
Tm_2O_3	n.a.	n.a.	n.a.	n.a.	n.a.	n.a.	n.a.	n.a.	n.a.	n.a.	n.a.	n.a.	n.a.	0.51	650
Yb_2O_3	b.d.	b.d.	b.d.	b.d.	b.d.	n.a.	b.d.	b.d.	b.d.	b.d.	b.d.	b.d.	b.d.	4.19	900
PbO	b.d.	0.09	b.d.	b.d.	b.d.	n.a.	0.45	0.35	b.d.	0.43	b.d.	0.10	0.13	b.d.	150
ThO_2	b.d.	0.30	0.76	4.23	8.77	0.03	0.73	0.46	0.76	0.41	4.01	b.d.	b.d.	b.d.	250
UO_2	b.d.	0.04	b.d.	0.07	0.11	n.a.	0.08	0.09	0.18	b.d.	0.94	b.d.	b.d.	0.06	200
F	n.a.	n.a.	n.a.	n.a.	n.a.	n.a.	1.31	1.42	1.53	0.95	n.a.	1.00	0.81	n.a.	1250
Cl	n.a.	n.a.	n.a.	n.a.	n.a.	n.a.	b.d.	b.d.	b.d.	b.d.	n.a.	b.d.	0.06	n.a.	400
$REE_2O_3 + Y_2O_3$	0.36	17.04	68.29	63.69	58.81	0.68	12.16	13.68	8.68	11.35	62.79	0.25	0.15	61.66	
Total	96.65	97.38	99.61	99.09	99.77	96.79	*97.56*	*97.69*	*96.98*	*98.24*	100.76	*99.05*	*99.10*	97.19	
Mineral	Apatite	Allanite		Monazite		Apatite		Bearthite		Sr-Bearthite	Monazite	Bearthite	Sr-Bearthite	Xenotime	
Normalised to	25 O	25 O		16 O		25 O		17 O		17 O	16 O	17 O	17 O	16 O	
P	6.035	0.008	3.983	3.960	3.911	5.965	3.948	3.941	3.953	3.976	4.017	3.997	3.999	4.014	
Si	b.d.	6.017	0.035	0.066	0.146	0.013	0.052	0.059	0.047	0.024	0.035	b.d.	b.d.	b.d.	
Ti	n.a.	0.007	n.a.	n.a.	n.a.	n.a.	n.a.	n.a.	n.a.	n.a.	n.a.	n.a.	n.a.	n.a.	
Al	b.d.	4.939	b.d.	b.d.	b.d.	b.d.	1.501	1.472	1.637	1.494	b.d.	2.014	2.006	b.d.	
Fe	0.006	1.073	b.d.	b.d.	b.d.	b.d.	b.d.	b.d.	b.d.	b.d.	b.d.	0.006	0.003	b.d.	
Mn	n.a.	b.d.	n.a.	n.a.	n.a.	n.a.	b.d.	b.d.	b.d.	b.d.	n.a.	n.a.	n.a.	n.a.	
Mg	n.a.	0.199	n.a.	n.a.	n.a.	0.531	0.528	0.581	0.406	0.524	n.a.	0.049	0.020	b.d.	
Ca	9.856	2.628	0.055	0.171	0.277	9.299	2.879	2.940	3.450	1.908	0.276	2.673	2.018	0.010	
Sr	n.a.	n.a.	n.a.	n.a.	n.a.	0.164	0.447	0.322	b.d.	1.473	n.a.	1.019	1.779	b.d.	
Y	b.d.	b.d.	b.d.	b.d.	b.d.	n.a.	0.003	0.007	0.032	b.d.	0.074	b.d.	b.d.	3.355	
La	0.005	0.266	1.052	0.842	0.672	0.008	0.122	0.155	0.075	0.142	0.854	0.002	b.d.	b.d.	
Ce	0.008	0.529	1.976	1.764	1.554	0.015	0.246	0.280	0.158	0.260	1.637	0.004	0.003	b.d.	
Pr	b.d.	0.057	0.195	0.199	0.192	0.003	0.030	0.023	0.012	0.021	0.172	0.002	b.d.	b.d.	
Nd	0.009	0.207	0.621	0.752	0.790	0.006	0.089	0.098	0.060	0.084	0.595	0.002	0.002	b.d.	
Sm	b.d.	0.031	0.065	0.094	0.122	0.009	0.017	0.016	0.010	0.012	0.107	b.d.	b.d.	b.d.	
Gd	b.d.	0.008	0.017	0.024	0.034	b.d.	0.012	0.012	0.011	b.d.	0.066	b.d.	b.d.	0.011	
Tb	b.d.	0.004	b.d.	b.d.	b.d.	n.a.	b.d.	b.d.	b.d.	b.d.	0.008	b.d.	b.d.	0.011	
Dy	b.d.	b.d.	b.d.	b.d.	b.d.	n.a.	0.004	b.d.	0.005	b.d.	0.015	b.d.	b.d.	0.161	
Ho	b.d.	b.d.	b.d.	b.d.	b.d.	n.a.	b.d.	b.d.	b.d.	b.d.	b.d.	b.d.	0.001	0.061	
Er	b.d.	b.d.	b.d.	b.d.	b.d.	n.a.	b.d.	b.d.	b.d.	0.002	b.d.	b.d.	b.d.	0.193	
Tm	n.a.	n.a.	n.a.	n.a.	n.a.	n.a.	n.a.	n.a.	n.a.	n.a.	n.a.	n.a.	n.a.	0.021	
Yb	b.d.	b.d.	b.d.	b.d.	b.d.	n.a.	b.d.	b.d.	b.d.	b.d.	b.d.	b.d.	b.d.	0.171	
Pb	b.d.	0.004	b.d.	b.d.	b.d.	n.a.	0.014	0.011	b.d.	0.014	b.d.	0.003	0.004	b.d.	
Th	b.d.	0.012	0.027	0.152	0.313	0.001	0.019	0.012	0.019	0.012	0.140	b.d.	b.d.	b.d.	
U	b.d.	0.002	b.d.	0.003	0.004	n.a.	0.002	0.002	0.005	b.d.	0.032	b.d.	b.d.	0.002	
F	n.a.	n.a.	n.a.	n.a.	n.a.	n.a.	0.249	0.269	0.274	0.189	n.a.	0.178	0.152	n.a.	
Cl	n.a.	n.a.	n.a.	n.a.	n.a.	n.a.	b.d.	b.d.	b.d.	b.d.	n.a.	b.d.	0.006	n.a.	
OH							1.751	1.730	1.725	1.807		1.819	1.842		
Sum Cations	15.930	15.990	8.028	8.028	8.014	16.016	9.917	9.934	9.881	9.953	8.029	9.777	9.840	8.013	
						P+Si = 6	P + Si = 4					P + Si = 4			
							OH + F + Cl = 2					OH+F+Cl = 2			

←*Tab. 1* Electron microprobe analyses of samples Mo9801, 85DM45a, and B8485A. n.a. = not analysed; b.d. = below detection limit. Detection limits (D.L.) at the two sigma level were derived for analytical settings of 20 kV and 15 nA, using peak and background settings as given in SCHERRER et al. (2000). The formula used was: D.L. (2σ) in ppm = $10^4 \times 2.241 / (t_{tot.} \times I_{pk} \times I_{pk} / I_{bgd})^{1/2}$ where $t_{tot.}$ = total integration time in seconds, I_{pk} = intensity on pure peak in counts per second, and I_{bgd} = intensity on background in counts per second. Italic numbers indicate totals corrected for F and Cl.

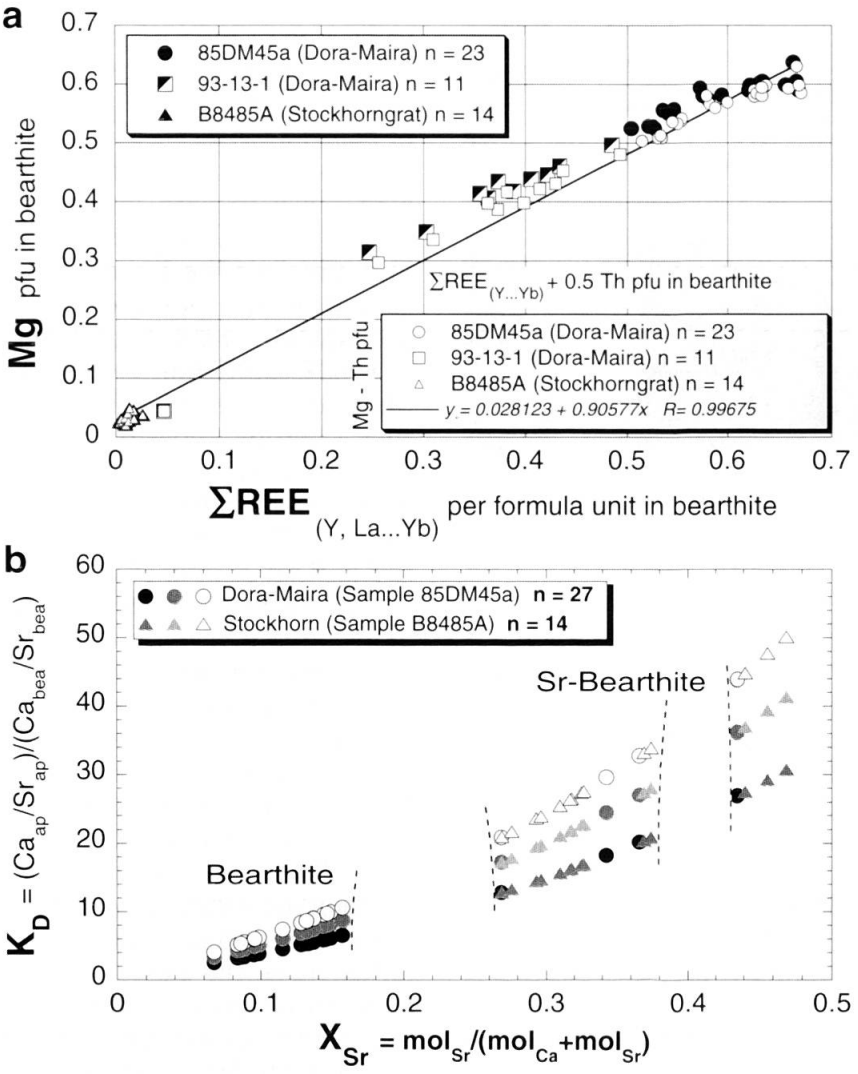

Fig. 4 (a) This plot displays the distinctive compositional difference between bearthite from the Dora-Maira (circles and squares) and bearthite from the Stockhorngrat (triangles). The relationship between Mg versus $\Sigma REE_{(Y, La...Yb)}$ in bearthite suggests an allanite-type $Ca_{-1}Al_{-1}MgREE$ substitution. An additional correction for a $ThMgREE_{-2}$ exchange, plotted as (ΣREE + 0.5 Th) versus (Mg–Th) and shown as open symbols, improves the fit to a 1:1 relationship. (b) X_{Sr} of coexisting Ca- and Sr-enriched bearthtites (85DM45a; B8485A) hinting at possible compositional gaps in the Ca–Sr bearthite series solid solution. The data represent analyses made on areas with different contrast of the BSE image seen within the $(Ca,Sr)_2Al(PO_4)_2(OH)$ phase (Figs 1a, 5).

mated volume proportions derived from image analysis are 70–80% apatite, and 20–30% monazite. In combination with the microprobe data the reaction coefficients are:

$$7Bea \rightarrow \sim 2.8Ap + 2Mnz + \sim 4.4Al_2O_3 + Ca_1Sr_1Al(PO_4)_2(OH) + H_2O.$$

Monte Rosa nappe (Mo9801): In this sample, a garnet-bearing mica gneiss free of Al-silicate minerals, zones consisting of apatite + monazite + corundum occur in the central part of a one millimetre-sized allanite porphyroblast (Fig. 2; note that the cut was arbitrary and thus may not represent the true 3D situation!). Allanite is virtually absent within these zones. For mass-balance estimates, ten areas free of allanite were selected within the reaction zones. The approximate volume ratios of the minerals are 50–70% apatite to 20% monazite to 10–30% corundum. This is similar to the first

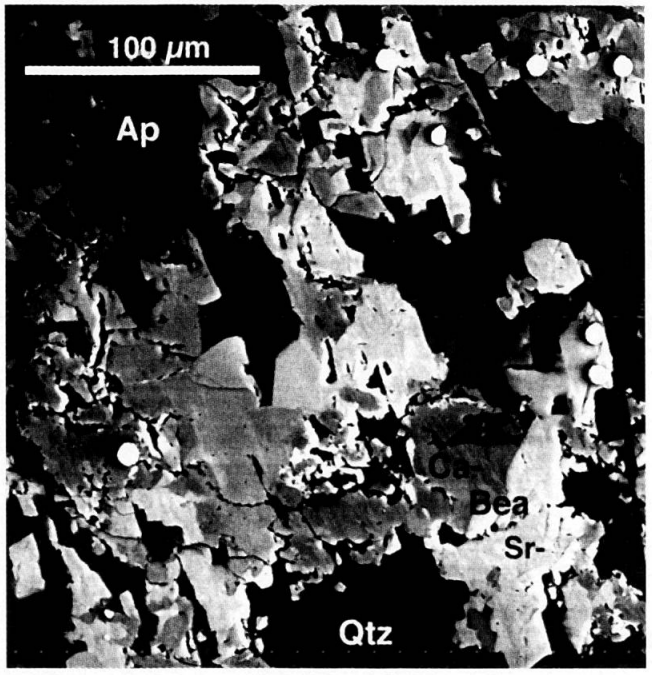

Fig. 5 BSE image of the Stockhorn sample (B8485A) displaying the patchy character of bearthite in this sample with Ca-enriched (darker) versus Sr-enriched (lighter) zones.

example, except for the presence of corundum. The REE and Th contents of the allanite grain are typically a quarter to one third of those in monazite from the symplectite (Figs 3b, e). However, there is no mineral phase within the symplectite containing Si or Fe, two major components of the enclosing allanite.

Stockhorngrat (B8485A): The third sample, described by BEARTH (1952), displays two compositionally different strontian bearthites coexisting with xenotime (Tab. 1; Fig. 4a), in the absence of monazite. The existence of Ca-rich (dark) versus Sr-rich (light) zones with distinct boundaries within the strontian bearthite (Fig. 5) match the observation made in the Dora-Maira sample 85DM45a (Fig. 1a), in which bearthite and strontian bearthite coexist side by side.

Discussion

This research on bearthite had two main interests: first, there is only limited knowledge on the formation of monazite, despite its importance as a popular time-constraint. The direct observation of a partially completed reaction involving bearthite and monazite has not been previously documented. Second, bearthite may contain considerable amounts of ThO_2 (Tab. 1) and thus offers an additional radiometric clock. If bearthite forms under ultra-high pressure conditions, the time when such conditions were reached might be constrained. Dating of symplectitic monazite surrounding such high P bearthite would then constrain the onset of decompression.

CHOPIN et al. (1993) suggested the symplectitic rim around bearthite to be a retrogressive decompression-related feature, and assumed bearthite to be a very high-pressure phase, because of its presence in coesite-bearing rocks (CHOPIN et al., 1991). However, subsequent experimental studies of bearthite (BRUNET and CHOPIN, 1995) showed that end-member bearthite is stable from ultra-high down to very low pressures in the CaO–Al_2O_3–P_2O_5–H_2O system. Bearthite breaks down to apatite + α-berlinite ($AlPO_4$) + corundum + vapour, with a positive Clapeyron slope, at approximately 550 °C at near-atmospheric pressure, to 800 °C at 8 kbar. P-T estimates for the Dora-Maira occurrence are about 725 °C and 30 kbar (talc + pyrope + coesite/quartz). P-T estimates for the Monte Rosa nappe, based upon the presence of talc + chloritoid + kyanite assemblages, range from 500 °C at 16 kbar (CHOPIN and MONIE, 1984) to 520 °C at 23 kbar (LE BAYON et al., 2001). Thus, while bearthite has been shown to be stable down to low pressures in the laboratory, so far, field descriptions of bearthite come all from allanite-free high pressure rocks.

The existence of strontian bearthite patches (Figs 1a, 5) suggests that excess strontium from bearthite apparently cannot be incorporated into the product apatite (SrO of apatite ranges from 1.7 to 3.5 wt%), nor accommodated by residual reactant bearthite. Concerning the Dora-Maira sample, this indicates either very slow Ca/Sr interdiffusion, or the existence of compositional gaps between bearthite and strontian bearthite under the conditions at which the symplectite formed (Fig. 4b). The REE contents of strontian bearthite and bearthite (Tab. 1; Figs 3a, d) are similar. Because neither monazite nor apatite contain Al, and no additional Al-phase is present within the symplectite, it appears that excess Al (± Mg) was removed with the fluid and either formed phengitic white mica or reacted with quartz to form kyanite, as was suggested by BRUNET and CHOPIN (1995). Nevertheless, the texture clearly shows that bearthite is the reactant in a monazite-forming reaction.

The Monte Rosa sample (Mo9801) is likely to have gone through high pressure at initially low temperature conditions during continental subduction of the Monte Rosa nappe (e.g., CHOPIN and MONIE, 1984; DAL PIAZ and LOMBARDO, 1986; LE BAYON et al., 2001). Because the assemblage contains abundant quartz, it is likely that bearthite relics survived only as inclusions, e.g. in al-

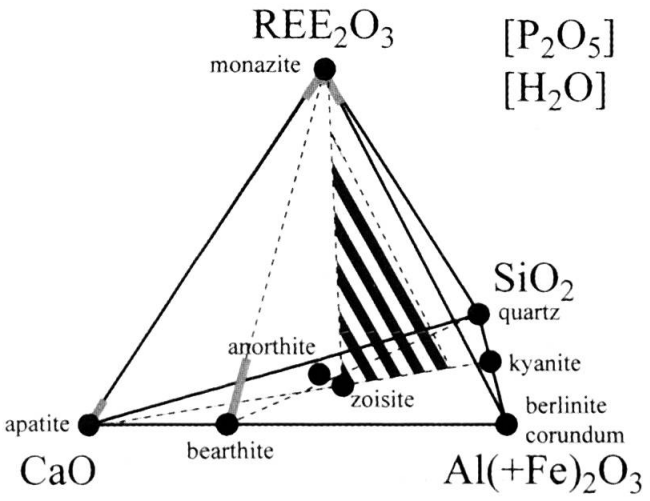

Fig. 6 Phase relations in the $CaO–Al_2O_3–SiO_2–REE_2O_3–P_2O_5–H_2O$ system projected from H_2O and P_2O_5. Shaded area indicates allanite solid-solution field.

lanite grains. During decompression, those bearthite relics broke down to an Ap + Mnz + Crn symplectite, similar to the Dora-Maira sample. Corundum, as observed in Fig. 2, could only survive because the Al-phase was isolated from quartz (shielded by the surrounding allanite) and thus was physically prevented from forming Al-silicate. The similar REE distribution patterns of allanite and monazite (Fig. 3b, e) suggest that they either have the same source of REE, or one grew at the expense of the other. The absence of an Fe-bearing silicate phase within the symplectite combined with the textural morphology, however, indicate that monazite is unlikely to have grown at the expense of the allanite. The presence of corundum within the symplectite suggests that bearthite was first, then overgrown by allanite, and the relic bearthite inclusions in allanite finally transformed into the monazite-bearing symplectite. Integrating the symplectite chemistry results in a bearthite composition. The phengitic composition ($Si_{3.40}$) of the white mica inclusion in the core of the allanite grain (Fig. 2), as opposed to a muscovite composition ($Si_{3.05}$) of the white mica in the matrix, supports a considerable pressure difference between matrix and inclusions.

ZHANG et al. (1997) and LIOU and ZHANG (1998) described monazite exsolution lamellae in apatite from the Dabie Shan ultra-high-pressure terrane. Similar exsolution of monazite in apatite has been observed by the third author in coesite-bearing rocks of Dora-Maira and by HARLOV et al. (2001) in the Kiirunavaara apatite iron ore. This may signify limited solid solution between monazite and apatite (Fig. 6). ZHANG et al. (1997) and LIOU and ZHANG (1998) also describe monazite as matrix grains, which suggests that either the Ca/Al ratio of the whole rock or the local Ca/Al ratio control the phosphate assemblage (Fig. 6). In calcium-rich rocks, apatite or $apatite_{ss}$ + $monazite_{ss}$ form, whereas in aluminium-rich rocks (pelitic rocks, and granitic gneisses) bearthite should be present (Fig. 6).

We furthermore propose that compositional, or miscibility(?), gaps may exist between bearthite and strontian bearthite (Fig. 4b). Xenotime (YPO_4) is known to fractionate heavy REE as opposed to light REE-dominant monazite (HEINRICH et al., 1997). Bearthite and strontian bearthite from the Stockhorn locality contain little REE and Mg (Figs 3c, 4a). In contrast, bearthite and strontian bearthite from the Dora-Maira sample (85DM45a) have large Mg + REE contents and display REE patterns similar to allanite. This points to an allanite-type substitution of $Ca_{-1}Al_{-1}REEMg$ in the bearthite or strontian bearthite structure (Fig. 4a). However, the data for the Dora-Maira samples plot slightly above the 1:1 line. If the data is additionally corrected for a $ThMgREE_{-2}$ exchange and then plotted as (ΣREE + 0.5 Th) versus (Mg–Th), shown as empty symbols in Fig. 4a, a ~1:1 relationship is obtained. Neither bearthite nor strontian bearthite in the Stockhorn sample (B8485A) appear to be monazite breakdown products. A potential preference of LREE over HREE within the bearthite or strontian bearthite crystal structure seems likely.

We suggest that the reason why bearthite, or symplectites replacing bearthite, are not often reported from high-pressure terranes is likely because bearthite is an accessory phase resembling monazite (or allanite, depending on composition) in thin section and thus may be overlooked.

Conclusions

A previously documented symplectite rim around a REE-bearing bearthite has been reinvestigated to confirm that: (1) the product phases are monazite + apatite, while the REE's are almost exclusively fractionated into monazite (Dora-Maira sample); (2) bearthite is a potential precursor of a fine-grained reaction texture of apatite + monazite + corundum (Monte Rosa sample); and (3) both bearthite and strontian bearthite are LREE-rich phases (Dora-Maira versus Stockhorn sample).

Considering the large number of studies based on radiometric dating of monazite, compared to a lack of knowledge of monazite-forming reactions, this work contributes to the understanding of the genesis of this mineral. Th–Pb (U–Pb) dating of

bearthite (1) and symplectitic monazite (2) might constrain the time: (1) when ultra-high-pressure conditions were attained (prograde); and (2) when decompression and/or heating began.

Acknowledgements

This study was part of first author's Ph.D. thesis supported by Schweizerischer Nationalfonds (grants# 20-49671.96/1 and 20-55306.98/1). The EMP laboratory at the MPI Bern has been funded by Schweizerischer Nationalfonds (Credit 21-26579.89). Beda Hofmann, Natural History Museum Bern, is thanked for providing the bearthite sample B8485A from the Stockhorngrat type locality. Open doors for use of the EMP facility at IMP Lausanne are also acknowledged. Andreas Jenni is thanked for his assistance with the SEM of the Geological Institute Bern. Critical reviews by J. Hanchar, S. Sorensen and R. Gieré are gratefully acknowledged.

References

AKERS, W.T., GROVE, M., HARRISON, T.M. and RYERSON, F.J. (1993): The instability of rhabdophane and its unimportance in monazite paragenesis. Chem. Geol., 110, 169–176.

BEARTH, P. (1952): Geologie und Petrographie des Monte Rosa. Beitr. geol. Karte Schweiz 96; Kümmerly & Frey AG, Bern.

BEARTH, P. (1957): Erläuterungen zu Blätter Saas und Monte Moro. Geologischer Atlas der Schweiz 1:25' 000; Blätter 30 und 31. Schweiz. Geol. Kommission, 1–20.

BINGEN, B., DEMAIFFE, D. and HERTOGEN, J. (1996): Redistribution of rare earth elements, thorium, and uranium over accessory minerals in the course of amphibolite to granulite facies metamorphism: The role of apatite and monazite in orthogneisses from southwestern Norway. Geochim. Cosmochim. Acta, 60, 1341–1354.

BORGHI, A., COMPAGNON, R. and SANDRONE, R. (1996): Composite P-T paths in the internal Penninic massifs of the western Alps: Petrological constraints to their thermo-mechanical evolution. Eclogae geol. Helv., 89, 345–367.

BOYNTON, W.V. (1984): Cosmochemistry of the rare earth elements: meteorite studies. In: P. HENDERSON [ed.]: Rare earth element geochemistry. Elsevier, Amsterdam, 63–114.

BROSKA, I. and SIMAN, P. (1998): The breakdown of monazite in the West-Carpathian Veporic orthogneisses and tatric granites. Geol. Carp., 49, 161–167.

BRUNET, F. and CHOPIN, C. (1995): Bearthite, $Ca_2Al(PO_4)_2OH$: stability, thermodynamic properties and phase relations. Contrib. Mineral. Petrol., 121, 258–266.

CHOPIN, C. and MONIE, P. (1984): A unique magnesiochloritoid-bearing, high-pressure assemblage from the Monte Rosa massif, western Alps: petrologic and $^{40}Ar/^{39}Ar$ study. Contrib. Mineral. Petrol., 87, 388–398.

CHOPIN, C., HENRY, C. and MICHARD, A. (1991): Geology and petrology of the coesite-bearing terrain, Dora-Maira Massif, western Alps. Eur. J. Mineral., 3, 263–291.

CHOPIN, C., BRUNET, F., GEBERT, W., MEDENBACH, O. and TILLMANNS, E. (1993): Bearthite, $Ca_2Al[PO_4]_2(OH)$, a new mineral from high-pressure terranes of the western Alps. Schweiz. Mineral. Petrogr. Mitt., 73, 1–9.

DAL PIAZ, G.V. and LOMBARDO, B. (1986): Early Alpine eclogite metamorphism in the Penninic Monte Rosa – Gran Paradiso basement nappes of the northwestern Alps. In: EVANS, B.W. and BROWN, E.H. (eds): Blueschists and eclogites. Mem. Geol. Soc. Am., 164, 249–265.

FINGER, F., BROSKA, I., ROBERTS, M.P. and SCHERMAIER, A. (1998): Replacement of primary monazite by apatite-allanite-epidote coronas in an amphibolite facies granite gneiss from the eastern Alps. Am. Mineral., 83, 248–258.

HARLOV, D., ANDERSSON, U. and NYSTRÖM, J.O. (2001): Apatite-monazite relations in the Kiirunavaara apatite iron ore, northern Sweden. Strasbourg, Journal of Conference Abstracts, 6, 683.

HEINRICH, W., ANDREHS, G. and FRANZ, G. (1997): Monazite-xenotime miscibility gap thermometry. 1. An empirical calibration. J. metamorphic Geol., 15, 3–16.

KINGSBURY, J.A., MILLER, C.F., WOODEN, J.L. and HARRISON, T.M. (1993): Monazite paragenesis and U–Pb systematics in rocks of the eastern Mojave Desert, California, U.S.A.; implications for thermochronometry. Chem. Geol., 110, 147–167.

LE BAYON, R., DE CAPITANI, C., CHOPIN, C. and FREY, M. (2001): Modelling Equilibrium Phase Diagrams for White Schists: New Insights on Metamorphic Evolution in the Western Penninic Alps. Strasbourg, Journal of Conference Abstracts, 6, 346.

LIOU, J.G. and ZHANG, R.Y. (1998): Petrogenesis of ultrahigh-P garnet-bearing ultramafic body from Maowu, the Dabie Mountains, Central China. Island Arc, 7, 115–134.

PAN, Y. M. (1997): Zircon- and monazite-forming metamorphic reactions at Manitouwadge, Ontario. Can. Mineral., 35, 105–118.

SCHERRER, N.C., ENGI, M., GNOS, E., JAKOB, V. and LIECHTI, A. (2000): Monazite analysis; from sample preparation to microprobe age dating and REE quantification. Schweiz. Mineral. Petrogr. Mitt., 80, 93–105.

SMITH, H.A. and BARREIRO, B. (1990): Monazite U–Pb dating of staurolite grade metamorphism in pelitic schists. Contrib. Mineral. Petrol., 105, 602–615.

ZHANG, R.Y., HACKER, B. and LIOU, J.G. (1997): Exsolution in ultrahigh-pressure rocks from the Dabie-Sulu (China) and Kokchetav (Khazakhstan) terranes. Terra Nova, 9, 43.

Manuscript received December 1, 2001; revision accepted November 5, 2001.
Editorial handling: R. Gieré